On-Line Aspects of Stereophotogrammetric Processing of SPOT Images

V. Kratky
Canada Centre for Mapping, 615 Booth Street, Ottawa, Ontario K1A 0E9, Canada

ABSTRACT: Several aspects must be considered when processing dynamic, time-dependent satellite imagery, such as produced by the SPOT system, in an on-line environment of photogrammetric compilation. Two major problems arise:

- the computer control of image stage positioning must cope with dynamic changes in the position and attitude of the imaging sensor and still retain its needed real-time performance; and
- in the continuous compilation mode, the model heights entered on input must be defined with respect to the curvilinear coordinate system of the ellipsoidal or geoidal surface.

These and some other related issues are addressed and solutions presented, based on extensive software simulations, on analysis of numerous experiments, and on practical testing in an analytical plotter.

INTRODUCTION

BACKGROUND INFORMATION on the SPOT satellite mission, its goals, and its technical parameters is available in numerous publications; here we refer to Chevrel and Weill (1981). Even before the satellite was launched in 1986, many studies analyzed the SPOT potential in the context of cartography and photogrammetry, particularly for topographic mapping. Out of existing, commercially available photogrammetric hardware, on-line photogrammetric systems are the only ones capable of handling the dynamic geometry of satellite imagery. Considerable research has been carried out to demonstrate this potential by adapting analytical plotter software for accurate geometric processing of SPOT imagery, as reported by de Masson d'Auteme (1980), Egels (1983), Dowman and Gugan (1985), Konecny *et al.* (1987), and Kratky (1987, 1988).

The geometry of SPOT and other satellite imageries based on the "push broom" principle differs significantly from that of photogrammetric frame cameras because their instantaneous optical imaging is restricted to a single plane containing the linear sensor. Two-dimensional image coverage is achieved by a consecutive digital collection of individual scanlines at a frequency corresponding to the scanning resolution within the lines. Thus, the two-dimensional image is constructed as an indefinitely long strip covering the ground swath under the orbit. The constant frequency of scanning causes the image coordinate y', measured along the strip, to become actually a measure of time. Individual SPOT image scenes are arbitrarily selected segments of the inherently continuous imagery. In contrast to frame cameras, which preserve the same orientation of the three-dimensional bundle of imaging rays for the whole frame, the spatial position and orientation of the imaging sensor is continually changing along the orbit and the imaging geometry becomes dynamic and time-dependent.

A rigorous geometric reconstruction of spatial relations between images and the ground scene must combine the principles of photogrammetric bundle formulation, modified in a time-dependent mode, with additional constraints derived from known orbital relations. An important objective of the solution is to properly derive and mathematically model all inherent variations in the position and attitude of the imaging sensor.

The dynamic character of imaging has its repercussions also in the process of photogrammetric compilation of SPOT images in on-line analytical instruments. The control of image positioning must effectively replicate the dynamic changes in the position and attitude of the sensor and still retain its needed real-time performance. The volume of calculations needed to update the projection center positions and the rotation matrices involved may increase the duration of the real-time programming cycle beyond acceptable limits, unless certain time saving modifications to some of the photogrammetric algorithms are applied. Special considerations must be given to the way in which the elevations are controlled in continuous compilation of contours. The standard photogrammetric footwheel control of the measuring mark maintains a constant height in a rectangular coordinate system, while in SPOT processing it must be continuously defined with respect to the curved ellipsoidal or geoidal surface. Finally, there are some peculiarities involved in stereoviewing of SPOT uncorrected, raw images (produced at SPOT Image level 1a) which are needed in a rigorous photogrammetric approach.

All these aspects are considered here in the context of formulation given by Kratky (1987) and with the use of the NRC Anaplot I on-line system.

REAL-TIME POSITIONING

Principles of Real-Time Positioning

On-line photogrammetric systems are coordinate measuring devices interfaced with a computer which can process measured information on-line with its collection. Of interest here are only closed-loop systems which not only instantly process the information, but also use it in a feedback mode to monitor and control the operation. The main element of this function is a continuous, computer-controlled real-time positioning of images. The positioning is achieved by digital means applicable to discrete points only and, in a continuous dynamic operation, it must appear physically smooth even though it is implemented by a fast repetitive cycle of digital computations. These proceed in a stream of densely spaced discrete data points defined by the operator's control of the measuring mark in the observed optical stereomodel. The computations are based on transformations between object and image spaces with the use of previously derived parameters. Included in the computations are corrections for any physical image distortions. The practically required frequency of the real-time loop is between 50 to 100 Hz. The operator retains the physical and dynamic control of the system through input control elements and, with a perfect illusion of continuity, receives his feedback from stereoobservations of computer positioned image details.

Real-Time Positioning of Photogrammetric Frame Images

Conventional photogrammetric images are taken by frame cameras specially calibrated to provide an image geometrically

PHOTOGRAMMETRIC ENGINEERING AND REMOTE SENSING,
Vol. 55, No. 3, March 1989, pp. 311–316.

0099-1112/89/5503–311$02.25/0

representing a point-by-point, straight-line projection of the object by a perspective bundle of rays passing through an ideal projection center. The projection center has coordinates X_c, Y_c, Z_c and the angular orientation of the bundle is defined by rotation matrix **M**. The basic form of an algorithm which relates the individual image and photogrammetric model points is fairly simple: orthogonal transformation of rectangular coordinates of a point from one space to the other is followed by auxiliary scaling.

For image coordinates x', y', principal distance f, and model coordinates X, Y, Z the projection from model to image, MDL-IMG: $(X,Y,Z) \vdash (x',y')$, is uniquely defined and implemented by a sequence of equations

$$\text{MDL-IMG:} \quad \begin{pmatrix} U \\ V \\ W \end{pmatrix} = \mathbf{M}^{\mathrm{T}} \begin{pmatrix} X - X_c \\ Y - Y_c \\ Z - Z_c \end{pmatrix}, \qquad s = -f/W, \begin{pmatrix} x' \\ y' \\ -f \end{pmatrix} = s \begin{pmatrix} U \\ V \\ W \end{pmatrix}, \quad (1)$$

while the opposite projection, IMG-MDL: $(x',y',f) \vdash (X,Y,Z)$, is obviously not unique and must be defined for a chosen level Z

$$\text{IMG-MDL:} \quad \begin{pmatrix} x \\ y \\ z \end{pmatrix} = \mathbf{M} \begin{pmatrix} x' \\ y' \\ -f \end{pmatrix}, r = (Z - Z_c)/z, \qquad \begin{pmatrix} X \\ Y \\ Z \end{pmatrix} = \begin{pmatrix} X_c \\ Y_c \\ Z_c \end{pmatrix} + r \begin{pmatrix} x \\ y \\ z \end{pmatrix}. \quad (2)$$

For future comparisons, it may be useful to establish the number of "hard" arithmetic operations (multiplications and divisions) involved in these basic transformations, while disregarding additional calculations needed to apply system corrections, fiducial transformation, interface functions, etc. Equations 2 include 13 of these operations: nine in matrix-vector multiplication, one division to derive scale r, and three scalar-vector multiplications. Equations 1 have only 12 hard operations, because scalar multiplication sW is not needed; resulting value $-f$ is already known.

In most cases the real-time program accepts X,Y,Z model coordinates as input and applies the MDL-IMG projection into both images, the resulting x',y',x'',y'' coordinates being used for the stage positioning

$$\begin{array}{ll} \text{RT:} & x'\ y' \leftarrow\!| \underline{X}\ \underline{Y}\ \underline{Z} \vdash\!\rightarrow x''\ y'' \\ & \qquad\quad \downarrow \\ \text{NRT:} & \qquad E\ N\ h \end{array} \quad (3)$$

The upper line represents the real-time (RT) transformations while the lower line indicates an optional computation for UTM coordinates of easting E and northing N, together with ellipsoidal or geoidal elevation h, which may proceed in near real time (NRT) when the positioning process is interrupted. The input values for the RT operation are underscored. The number of needed hard operations is $2 \times 12 = 24$.

In triangulation applications, however, a modified approach is more efficient. For instance, the operator's input is x',y',Z, which means that the handwheels operate directly on the left image and the projection proceeds as IMG1-MDL-IMG2

$$\begin{array}{ll} \text{RT:} & \underline{x'}\ \underline{y'}\ \underline{Z} \vdash\!\rightarrow X\ Y \vdash\!\rightarrow x''\ y'' \\ & \qquad\quad\ \downarrow \\ \text{NRT:} & \qquad E\ N\ h \end{array} \quad (4)$$

Here, the number of involved hard operations is $13 + 12 = 25$. Alternately, the right image may represent the primary input and the projection proceeds backwards as IMG2-MDL-IMG1. This arrangement is necessary in order to establish the known positions of tie points measured in preceding models of a bridging procedure. The practical effect of this mode of positioning is that it conveys an illusion of a stereocomparator operation in which elevation changes are interpreted as parallax displacements in one image only.

Real-Time Positioning of SPOT Images

The position of the projection center and the corresponding attitude matrix **M** are dependent on time and, therefore, can be expressed as functions of y'

$$\mathbf{X}_c = (X_c, Y_c, Z_c)^{\mathrm{T}} = F_c(y'), \ \mathbf{a} = (\kappa, \phi, \omega)^{\mathrm{T}} = F_a(y'), \ \mathbf{M} = F_M(\mathbf{a}). \quad (5)$$

Function F_M represents the construction of a rotation matrix from three parameters, and functions F_c, F_a can be expressed as quadratic polynomials, e.g.,

$$X_c = X_o + y'X + y'^2\ddot{X} + \ldots \text{ etc} \quad (6)$$

where X_o corresponds to the position for the centre of scene and $\dot{X}$ and $\ddot{X}$ are linear and quadratic rates of change, respectively. The volume of real-time computations is obviously high because of the need to steadily update F_c, F_a, and F_M. The projection from image to model is then represented by an expanded sequence of equations with input variables x',y',Z as in Equations 2

$$\text{IMG-MDL:} \quad \mathbf{x} = (x\ y\ z)^{\mathrm{T}} = \mathbf{M}(x'\ 0\ -f)^{\mathrm{T}}, \quad r = (Z - Z_c)/z, \ \mathbf{X} = \mathbf{X}_c + r\mathbf{x}, \quad (7)$$

where $\mathbf{X} = (X\ Y\ Z)^{\mathrm{T}}$.

The projection from model to image, MDL-IMG: $(X,Y,Z) \vdash (x',y')$, is even more complicated because functions F_c, F_a, F_M all depend on unknown y' which is to be derived in the same process. Consequently, the projection is not feasible in a single sequence of transformations as in Equations 1. An initial approximation of x',y' must be gradually refined by iterations which involve a repeated sequence of Equations 7 until all values $\mathbf{X}_c$, $\mathbf{a}$, x',y' stabilize and computed **X** agrees with that on input. The structure of this projection is as follows:

$$\begin{array}{l} \text{MDL-IMG: Estimate } x',y' \\ \quad \text{Repeat} \\ \quad\quad \text{IMG-MDL: } (x',y')_i \vdash (X,Y)_i, Z \\ \quad\quad d(x',y')_i = ((X,Y) - (X,Y)_i)/r \\ \quad\quad (x',y')_{i+1} = (x',y')_i + d(x',y')_i \\ \quad \text{Until } d(x',y')_i \text{ is negligible} \quad . \end{array} \quad (8)$$

The number of multiplications involved in Equations 7 is nine for each function F_c, F_a and about 24 in F_M, then six for the rotation and four for scaling of coordinates, the total being 52. On the average, Equations 8 may need to be repeated four times, yielding a total of 216 multiplications.

To reduce the need for excessive iterations, the real-time control of positioning should follow combination IMG1-MDL-IMG2 identified by the schematic (Equation 4), starting with x',y' coordinates of the left image on input and project them on a desired level Z in straightforward operations (Equation 7) first. The iterative process then applies only to the projection from model to the right image. However, even in this arrangement the number of multiplications per cycle is very high; using previous estimates for Equations 7 and 8, a total of 268

multiplications are used, which is about 11 times more than in positioning of conventional photogrammetric images.

Streamlining of Real-Time Programming Cycle for SPOT Images

Unless special arrangements to streamline the algorithms are found, the computation time used may be too high. An obvious option may be to resort to an assembly language coding which would cut down on run time. Yet, a higher level language programming is generally preferred for the convenience and flexibility of its use when changes are needed. Another possibility is to restrict the use of the double precision mode in computations to a minimum, where absolutely necessary. In SPOT transformations, the only operations and variables which warrant double precision are UTM conversions, geocentric coordinates, and related scale factors or conversion constants. None of these are needed in real-time computations and they can be run entirely in single precision, preserving six-digit accuracy. Obviously, any object time overhead will slow down execution of a program and, consequently, calls to subroutines should be avoided and replaced by their repeated direct coding in the real-time module. There is also a great potential for speeding up the real-time cycle by simplifying the transformations and running a fast, standard real-time program for conventional frame images, while compensating its systematic deficiencies. This is done by applying corrections taken, or interpolated, from look-up tables prepared in advance for the full spatial range of the ground scene, as described, e.g., by Konecny (1987). Yet another alternative consists in modeling the time demanding series of rigorous transformations by polynomial expansions, thus mapping the input values into any desired output. The accuracy of this process can be maintained at a proper level by empirical testing of the transformation degree and of the form and number of included terms, as needed. This approach will be demonstrated below in this paper.

It may be of interest to demonstrate some practical effects of streamlining with an example of an experimental series of refinements in the positioning algorithm, as implemented by the author. The schematic (Equation 4) carried out using the formulation of Equations 7 and 8 was programmed in Fortran 77, and the speed of the RT cycle was tested in a DEC VAX 750 computer by running batches of up to 1000 cycles at a time. With subroutines used for PHG-MDL conversion and for the construction of rotation matrices, and with all variables declared in double precision, a single RT cycle was measured to last 26.4 ms. After the subroutine calls for PHG-MDL were replaced by repeated direct coding, the time was reduced down to 8.1 ms. Further time reduction to 6.5 ms was achieved by reducing the effective size of matrix **M** in Equations 7 from 3 by 3 to 3 by 2. In the next step, all calls to subroutines were eliminated and dynamic conditions of continuous positioning were simulated by using results from a previous cycle as an approximation for the new cycle. Depending on the speed of simulated motion, the resulting cycle time was 3.8 or 2.8 ms for fast and slow positional changes in y' by 50 μm or 5 μm per cycle, respectively. Finally, with the whole RT program run in single precision, the cycle time was brought down to 3.1 and 2.1 ms, considering fast and slow motion, respectively. A significant total improvement by a factor of ten times was clearly demonstrated. Nevertheless, in spite of the relative improvement, there are still about 160 multiplications in each RT cycle. The same test program run on a PDP 11/45 minicomputer is about ten times slower, with 20 and 30 ms for the same above range of dynamic changes. Because the resulting RT frequency of 50 Hz is here just on the borderline of acceptability for an on-line operation, one more improvement was successfully tested. Repeated rigorous and computationally demanding constructions of orthogonal matrices from their three independent parameters were eliminated. Instead, each of the nine matrix elements was individually calculated from linear fitting functions prepared in advance. Because the matrix construction appears in the streamlined positioning cycle about three times, the saving amounted to 36 multiplications, so reducing their total number in the cycle to 124.

ON-LINE INPUT CONTROL

Control of Elevation Input

The task of using geoidal or ellipsoidal heights h on input to an analytical plotter involves their conversion to model coordinates Z by a series of rigorous and time consuming transformations described by Kratky (1987,1988). Unfortunately, their direct implementation is practically impossible in a real-time cycle with a frequency higher than 50 Hz.

Because earth curvature is well pronounced in a SPOT ground scene, geoidal or ellipsoidal elevations h must be measured or followed by the Z-wheel along curved surfaces characterized by constant h, as indicated in Figure 1. An efficient "h-to-Z" conversion is needed on input. It can be iteratively implemented starting with an initial approximation of Z, as follows

$$\begin{aligned} &h-Z\text{: Estimate } Z \\ &\quad \text{Repeat} \\ &\quad\quad (x',y',Z_i) \mapsto (X,Y,Z)_i \mapsto (E,N,h)_i \\ &\quad\quad Z_{i+1} = Z_i + h - h_i \\ &\quad \text{Until } h = h_i \end{aligned} \tag{9}$$

This transformation can be rigorously determined in advance for a suitable (5 by 5) square grid of values x',y' covering the left SPOT image, and for three levels of h extended over the full elevation range of the ground scene. Following that, a suitable polynomial function $F_Z(x',y',h)$ is derived to fit the spatial grid through a least-squares solution, so defining parameters which can then be applied in real-time conversions with enormous time savings. The degree of the transformation, the number and form of needed terms were determined experimentally and yielded the following expression:

$$\begin{aligned} Z &= F_Z(x',y',h) \\ &= (1\ h\ x'\ y'\ hx'\ x'y'\ x'^2\ y'^2\ hx'^2\ x'^3)\mathbf{p} = \mathbf{c}_Z^T\mathbf{p}_Z \end{aligned} \tag{10}$$

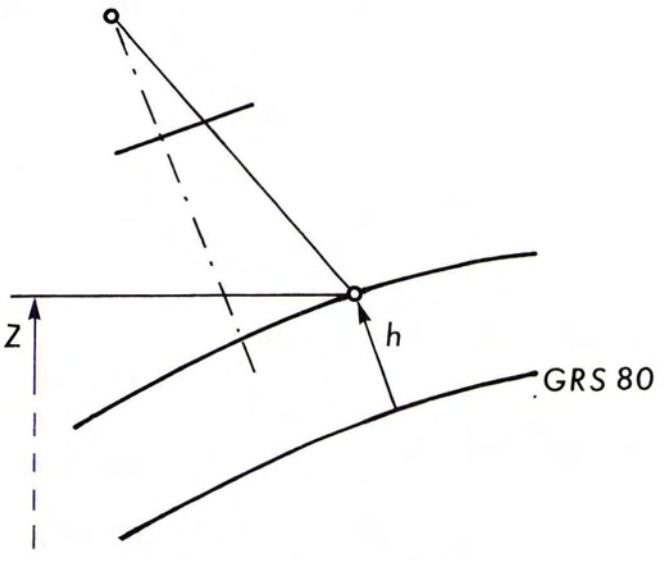

FIG. 1. Projection of imaging rays on reference ellipsoid.

where $\mathbf{p}_Z$ is a vector consisting of parameters p_1 to p_{10} and $\mathbf{c}_Z$ – vector of ten corresponding polynomial coefficients formed from chosen (x',y',h) power combinations. The number of multiplications in Equation 10 can be reduced from 17 to 9 by a proper grouping of terms; for instance,

$$Z = p_1 + h(p_2 + x'(p_5 + p_9x')) + x'(p_3 + x'(p_7 + p_{10}x')) + y'(p_4 + p_6x' + p_8y'). \quad (10a)$$

The formulation easily meets the real-time requirements and provides an excellent accuracy. Absolute errors of the transformation are within $|dZ| < 0.2$ m for the range of $\Delta h = 1$ km and within $|dZ| < 0.5$ m for $\Delta h = 4$ km, both cases being computed for the maximum side view angle 27° of the imaging sensor.

Using this approach, the schematic (Equation 4) for the real-time positioning of SPOT images should now be changed to a new form in which the number of needed multiplications increases from 124 to 133

$$\begin{array}{ll} \text{RT:} & \underline{x'}\ \underline{y'}\ \underline{h} \vdash\!\rightarrow X\ Y\ Z \vdash\!\rightarrow x''\ y'' \\ & \qquad\qquad\ \downarrow \\ \text{NRT:} & \qquad\qquad E\ N \end{array} \quad (11)$$

GENERALIZED CONTROL BY FITTING FUNCTIONS

The same principle of polynomial modeling can be applied to computations of other variables in the real-time process. The most useful application in this regard is its substitution for the rigorous composite transition from the left to right image, IMG1-MDL-IMG2. Experiments demonstrated an excellent performance of a single-step mathematical mapping with a 13-term polynomial for x'' and 11-term polynomial for y'': i.e.,

$$x'' = F_x(x',y',h) = \mathbf{c}_x^T\mathbf{p}_x \quad (12)$$

$$y'' = F_y(x',y',h) = \mathbf{c}_y^T\mathbf{p}_y \quad (13)$$

where

$$\mathbf{c}_x = (1\ h\ x'\ y'\ h^2\ hx'\ hy'\ x'y'\ x'^2\ y'^2\ x'^2y'\ x'y'^2\ hx'^2)^T \quad (12a)$$

$$\mathbf{c}_y = (1\ h\ x'\ y'\quad hx'\ hy'\ x'y'\ x'^2\ y'^2\ x'^2y'\ x'y'^2)^T \quad (13a)$$

and $\mathbf{p}_x$, $\mathbf{p}_y$ are corresponding vectors of parameters. Equations 12 and 13 were tested for stereopairs of SPOT images corresponding to ratio $b/h = 1.0$, that is, for the combination of maximum view angles $+27°$ and $-27°$. The accuracy is excellent for any practical range h, leaving maximum absolute errors within $|dx''| < 0.5$ μm and $|dy''| < 0.3$ μm. Similarly to the arrangement in Equation 10a, the number of multiplications for the 13-term polynomial expression in Equation 12 can be reduced from 24 to 12, and for y'' in Equation 13 from 19 to 10.

Quite logically, when already computing the raster of rigorous Z-values in Equations 9 needed for polynomial Equation 10, one can also store values X,Y and derive their corresponding fitting functions with 11-terms: i.e.,

$$X = F_x(x',y',h) = (1\ h\ x'\ y'\ hx'\ hy'\ x'y'\ x'^2\ y'^2\ hx'^2\ x'^3)\mathbf{p}_X = \mathbf{c}_X^T\mathbf{p}_X \quad (14)$$

$$Y = F_Y(x',y',h) = \mathbf{c}_X^T\mathbf{p}_Y \quad (15)$$

where $\mathbf{p}_X$, $\mathbf{p}_Y$ are 11-component vectors of parameters for the computation of X, Y, respectively. Parameter grouping similar to that of Equation 10a will allow conversions of X,Y to be implemented with only 10 multiplications each. The accuracy of these transformations is also excellent; maximum absolute errors in X and Y are smaller than 0.3 m for any practical range of elevations.

Eventually, the near real-time computation of UTM coordinates E,N can also be arranged by similar fitting functions of (x',y',h) to save computing time and to circumvent the computation of intermediate model values X,Y,Z. The above polynomial form of $\mathbf{c}_X$ was found adequate to implement the computation of E and N

$$E = F_E(x',y',h) = \mathbf{c}_X^T\mathbf{p}_E \quad (16)$$

$$N = F_N(x',y',h) = \mathbf{c}_X^T\mathbf{p}_N \quad (17)$$

with maximum absolute errors $|dE| < 1.1$ m and $|dN| < 0.4$ m for any range of elevations.

The concept of real-time positioning of images in analytical plotters can then be fully based on direct polynomial mapping of all needed conversions and the original schematics of consecutive projections (Equation 4 or 11) are replaced by a set of independent mapping functions

$$\begin{array}{lll} \text{RT:} & x'\ y'\ h & \vdash\!\rightarrow x''\ y'' \\ & [x'\ y'\ h & \vdash\!\rightarrow X\ Y\ Z] \\ \text{NRT:} & x'\ y'\ h & \vdash\!\rightarrow E\ N \\ & [X\ Y\ Z & \vdash\!\rightarrow E\ N\ ] \end{array} \quad (18)$$

relating that input image space to any other needed coordinate space through chosen elevation h. The two lines enclosed in brackets represent options. In this arrangement, the real-time positioning loop can be implemented with no compromise in rigor or accuracy with only 22 multiplications and is six times faster than that of the streamlined approach. Ultimately, its performance surpasses even that of the standard loop for frame images. For example, the PDP 11/45 controlled positioning loop for the Anaplot I improved its real-time frequency to 130 Hz. Table 1 presents an overview of the number of multiplications in individual cases discussed above.

Similar time saving considerations are also important for the environment of digital image analysis and processing systems where the real-time constraints of image matching, resampling, and transformations are even more critical. The approach of using mapping functions is directly applicable.

CHARACTER OF SPOT GEOMETRY

To demonstrate practically the relation of and the differences in two SPOT stereoimages of the same ground scene, an example of fictitious data was generated. The left image was chosen as vertical, the right image was oblique, pointed 25° due west, and the geographic latitude of the scene was $\phi = 46°$. In the left image considered in the physical size ($s = 78$ mm) of the sensor's linear array, a (5 by 5) square reference grid was adopted, which was projected first to a zero level of the GRS 80 reference ellipsoid and then back into the tilted right image, respecting the orbital motions of the satellite and an ideal attitude control of the sensor. Rigorous spatial transformations were applied throughout the calculations. The distorted grid pattern is nonlinear and corresponds to the effect of Equations 12 and 13. Figure 2 is a graphical representation of the square reference frame for the left image and of the distorted corresponding grid of the right image, when coordinate axes of both images are superimposed. The maximum absolute differences in coordinates of corresponding points are 10.6 mm for x' and 2.3 mm for y'. Local x- and y-segments of the reference grid are distorted in the right image, both in scale and rotation. The most noticeable is the change of x-scale causing image compression

TABLE 1. NUMBER OF MULTIPLICATIONS INVOLVED IN DIFFERENT RT FORMULATIONS

Process	Equations	Number
Standard RT Positioning – FRAME	(1)	24
Straight RT Positioning – SPOT	(7),(8)	268
Streamlined RT Positioning – SPOT	(7),(8)	124
Streamlined RT Positioning – SPOT	(7),(8),(10)	132
Generalized RT Positioning – SPOT	(12),(13)	22

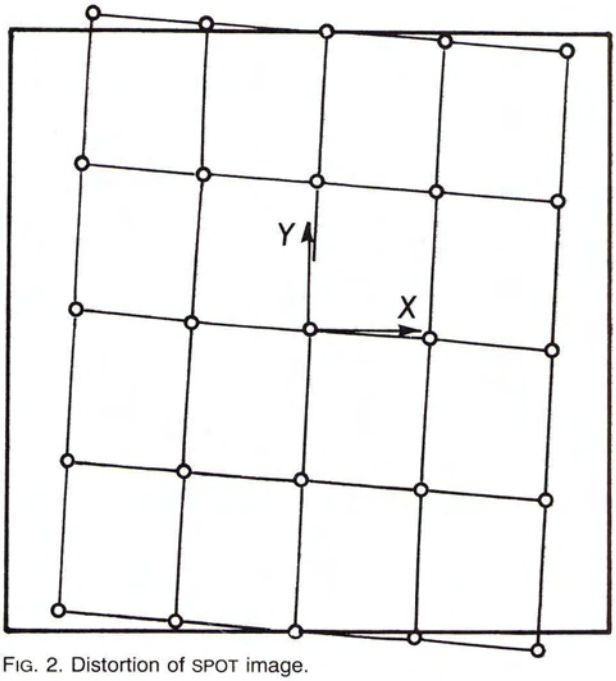

FIG. 2. Distortion of SPOT image.

TABLE 2. CHANGE IN GEOMETRY BY PROJECTING VERTICAL INTO OBLIQUE SPOT IMAGE

Change	Scale of Segments in x	Scale of Segments in y	Rotation of Segments in x	Rotation of Segments in y	Skew angle y-to-x
Minimum	0.767	1.000	−4.01°	−2.68°	1.12°
Average	0.795	1.000	−4.16°	−2.79°	1.37°
Maximum	0.823	1.000	−4.32°	−2.91°	1.61°

of 20 percent, while the y-scale is practically unchanged. Both x- and y-segments are rotated clockwise; however, the x-rotation is more pronounced and this results in a shearing effect, changing the original right angles of the grid. All these changes vary continuously. Table 2 summarizes the range of the variations and their average values. From the examples it can be deduced that for two oblique images their x-scales are practically identical, while the relative rotations and skew are approximately two times larger than for the tabulated case.

The range of the variable distortion is reasonably small and does not cause any special concerns with regard to the optical conditions of stereo observation of SPOT raw image transparencies. The viewing field rotation can be optically adjusted for the whole SPOT image and the remaining variations and skewness are not significant enough to affect the observation comfort. There is no need to apply computer control of visual field rotation available in some analytical plotters. Equal scale of y-segments warrants that no residual y-parallaxes will appear in the periphery of the optical field of view, when their centers are either manually adjusted or are under computer control.

The only serious practical problem arises from the x-scale compression of the tilted SPOT image, which considerably affects the stereo observations. As a result of the change in scale of two images which are supposed to be merged in the process of stereoperception, one perceives the increase of x-parallaxes towards the periphery of the viewing field and, as a result, the stereomodel becomes considerably slanted in the x-direction. As seen from Table 2, the variations of this scale change over the whole image area are only ±2.8 percent and, if the average x-scale were corrected when reproducing the transparencies, the problem would be resolved.

Figure 3 illustrates the conditions under which SPOT images may be taken. Ground segment D is projected into d' or d'' in a vertical or oblique image, respectively: i.e.,

$$d' = D \cdot f/h, \; d'' = D\cos^2 T \cdot f/h,$$

where f is the focal length of the imaging system and h is the flying altitude. Scale distortion m, causing x''-compression, can be estimated by comparing both image segments: i.e.,

$$m = 1 + dm = d''/d' = \cos^2 T = 1 - \sin^2 T. \qquad (19)$$

Scale error dm is always negative and is a function of tilt T of the sensor. Consequently, needed reproduction scale r or scale correction dr, to be applied during the reproduction process, can be derived as

$$r = 1/m = 1/\cos^2 T \quad \text{or} \quad dr = \tan^2 T. \qquad (20)$$

Obviously, the distortion is identical for positive or negative tilts of the same size and is not critical for the geometrically optimal, double convergent SPOT image pairs with base-to-height ratio of 1. However, it is the difference between the absolute values of tilts T which causes problems. Even then, scale errors of up to 5 percent, corresponding to $T = 13°$, can still be disregarded. In order to avoid difficulties with extreme vertical-oblique combinations, one should use transparencies whose x-scale is compensated at the time of their photo reproduction, as shown by Equation 20.

CONCLUSIONS

The dynamic character of SPOT images complicates the implementation of the algorithms for rigorous real-time positioning of image stages in on-line photogrammetric operations. The number of multiplications in a single real-time cycle is about 11 times higher than in conventional positioning of photogrammetric frame images. With special arrangements adopted in program coding and with some algorithmic modifications, the volume of multiplications can be reduced by more than 50 percent. A significant improvement is achieved through modeling of rigorous iterative transformations by a direct polynomial

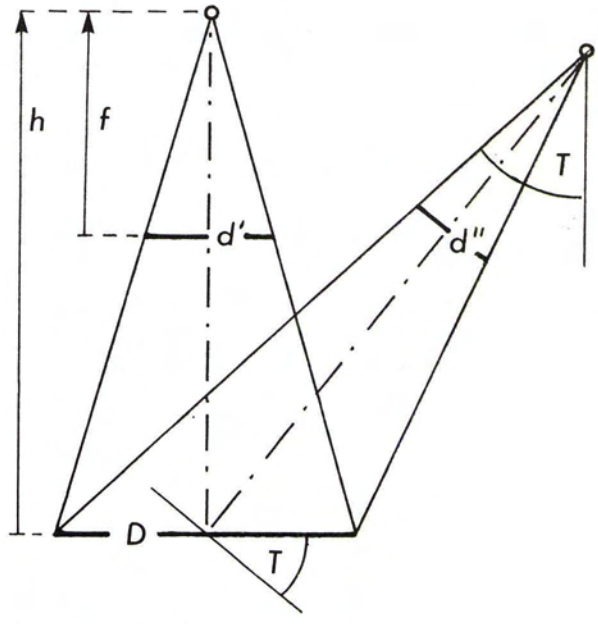

FIG. 3. Compression of oblique image.

mapping of "input-to-output" values. A concept of a generalized control of real-time operations for analytical on-line instruments, as well as for image processing systems, was developed and tested. With its use the real-time positioning cycle can be implemented with 22 multiplications only, i.e., even faster than using a standard cycle for frame cameras. The process is extended to control photogrammetric operations defined with respect to curved geodetic surfaces, as needed for measurements of ellipsoidal or geoidal heights.

REFERENCES

Chevrel, M., and G. Weill, 1981. The SPOT Satellite Remote Sensing Mission. *Photogrammetric Engineering and Remote Sensing*, 47(8):1163–1171.

Dowman, I. J., and D. J. Gugan, 1985. Application Potential of SPOT Imagery for Topographical Mapping. *Advanced Space Research*, 5(5):73–79.

Egels, Y., 1983. Amelioration des logiciels TRASTER: restitution d'images a géométrie non conique. *Bull. Inf. IGN*, 1983(2):19–22.

Konecny, G., P. Lohmann, H. Engel, and E. Kruck, 1987. Evaluation of SPOT Imagery on Analytical Photogrammetric Instruments. *Photogrammetric Engineering and Remote Sensing*, 53(9):1223–1230.

Kratky, V., 1987. Rigorous Stereophotogrammetric Treatment of SPOT Images. *SPOT 1—Utilisation des images, bilan, resultáts*, CNES, Paris, pp. 1281–1288.

———, 1988. Universal Photogrammetric Approach to Geometric Processing of SPOT Images. *International Archives of Photogrammetry and Remote Sensing*, 27(B4):180–189, ISPRS, Kyoto.

de Masson d'Autume, M.G., 1980. Le traitement géometrique des images de télédétection. *Annales des Mines* 1980(2):53–62.

(Received 25 October 1988; accepted 7 November 1988)

BOOK REVIEW

Remote Sensing Methods and Applications by R. Michael Hord. John Wiley & Sons, 605 Third Avenue, New York N.Y. 10158 - 0012. 1986, 362 pages 138 figures, 49 tables. Hard cover.

THIS BOOK, the second in the "Wiley Series in Remote Sensing," was written to redress a lack of collected pragmatic information and an absence of surveys of practical topics in digital image processing. As such, it is a compilation based on extracts from selected published papers and documents systematically arranged into a readable text. It is aimed at the experienced worker in the field of digital image processing of remotely sensed data, and the material is presented at a level that presumes familiarity with topics normally considered in an introductory text.

The book has three main chapters covering sensors, digital processing and analysis techniques, and applications. Chapter One discusses four sensor systems in detail: radars (aircraft and spacecraft), CZCS, Landsat TM, and RBV. Much of the information has been collated from NASA reports, including many which are often not seen by workers on the periphery of the technology. Discussion on the way in which the various sensing systems operate is illustrated by diagrams and schematics. To the image processing specialist such background can provide valuable insights to understanding the type of data produced by various sensing systems. Discussion of the Landsat MSS would have seemed more appropriate than the RBV; however, the author does draw attention to the fact that a very large collection of RBV digital data exists that may be usefully processed by current techniques. Following the discussion on each sensor there is a brief two-page review of the system. The chapter concludes with a similar brief overview (approximately one page each) of 11 future sensing systems. These cover VISSR Atmospheric Sounder, AVHRR, SIR-B, Multispectral Linear Array, Shuttle TIMS, Ocean Color Imager, Shuttle Imaging Spectrometer, Imaging Spectrometer, Multifrequency Lidar Facility, SPOT, and EOS. More detail on some of these, and other, instruments would be useful though, as the author points out, an exhaustive coverage would be too voluminous and those included have been selected to convey the growth directions and time scales of the technology.

Chapter Two has eight sections covering aspects of more advanced processing and analysis of digital data. The author notes that the processing approaches discussed are intended to provide insights on how some persistent problems may be attacked in novel ways. Though the reader is unlikely to want to try them all, they demonstrate interesting approaches which may stimulate investigations in related directions.

The last chapter discusses application in four discipline areas: meteorology, geology, agriculture, and maritime. Workers in other disciplines not covered here should not be discouraged from reading this book because the approaches adopted for data manipulation and information extraction can provide stimulating reading irrespective of discipline. Remote sensing applications will continue to expand, and innovation will be assisted by mulitdisciplinary cross-fertilization of ideas.

Overall, this volume pulls together a useful cross-section of information. For those who have entered remote sensing in the 1980s, one of the strengths of this book is the collation into one volume of much basic information on remote sensing systems published prior to that time. Such information is often taken for granted as being common knowledge but may not be known unless individuals make a deliberate effort to search out the data. A printing deficiency noted in the review copy was that reproduced imagery (black and white) has a tendancy to be darker than normal.

I recommend the volume as a very useful collation of particular value to lecturers in remote sensing and/or image processing, and to those who have become involved in image processing from computing or electronics backgrounds with only limited study of sensor systems or applications. It would also serve as a text for a second course in a university program on remote sensing and for industry-oriented intensive short courses on the topic.

—Colin J. Simpson
Division of Petrology and Geochemistry
Bureau of Mineral Resources
Canberra, A.C.T. Australia